Current Applied Physics 17 (2017) 1260–1263

Contents lists available at ScienceDirect

Current Applied Physics

journal homepage: www.elsevier.com/locate/cap

Triple-band metamaterial absorber based on single resonator

Young Ju Kim [a], Ji Sub Hwang [a], Young Joon Yoo [a], Bui Xuan Khuyen [a], Xianfeng Chen [b], YoungPak Lee [a,*]

[a] Department of Physics, Quantum Photonic Science Research Center and RINS, Hanyang University, Seoul, 133-791, South Korea
[b] Shanghai Jiaotong University, Shanghai, China

ARTICLE INFO

Article history:
Received 28 February 2017
Accepted 19 June 2017
Available online 20 June 2017

Keywords:
Metamaterials
Resonance
Subwavelength structures
Nanostructures absorption

ABSTRACT

The single resonator generally reveals a single absorption band, and the resonators with different sizes or shapes have to be arranged in order to achieve multi-absorption bands. We propose the triple-band metamaterial absorber by utilizing only single resonator. Meta-atoms are made of the toothed-wheel shape metallic pattern and a continuous metallic plane, separated by a dielectric layer. The first and the third absorption bands are induced by the fundamental and the third-harmonic magnetic resonances, respectively, and the second absorption band is induced by the magnetic resonance relevant to two grooves. In addition, the diffraction peak appears between the second and the third absorption bands, due to the surface currents which are separated between the upper and the lower metallic pattern parts. The proposed structure is scalable to smaller size for the infrared and the visible regimes.

1. Introduction

Metamaterials (MMs) mean artificial materials to obtain the properties, which cannot appear in nature, such as extraordinary optical transmission [1], and negative refraction index [2]. The electric permittivity and the magnetic permeability of materials, with respect to incident electromagnetic (EM) wave, can be adjusted by the sophisticated structure and the proper structural parameters of MMs. A lot of researchers have been involved in studying MMs due to a wide range of prompt and probable applications, for instance, cloaks [3], super lens [4], and absorbers from radio [5] to the optical frequencies [6] and for nearly every band in-between [7,8]. MM perfect absorbers (MMPAs) can be useful in many fields, such as solar energy [9], plasmonic sensors [10], bolometers [11] and photo-detectors [12]. Since MMPA was introduced [13], many kinds of MMPAs have been investigated: multi-band [14,15], broadband [16], switchable [17], and polarization- [18] and incident-angle- [19] insensitive MMPAs. Conventional MMPAs are made of a metallic pattern on one side and a continuous metallic plane on the other side, separated by a dielectric layer. The metallic pattern belongs to the suppression of the reflection by using the same impedance as free space, and the continuous metallic plane serves obstruction of the transmission. In comparison with the single-band high performance, multi-band high absorption is in highly desired in the sense of application perspective. The structures of MMPA have become complicated in order to achieve multi-band, such as double- [14], triple-loop [15], donut type [18] and bar by using the fundamental and the third-harmonic resonances [20]. In this work, we demonstrate the tunable triple-band MMPA, based on the simple toothed-wheel structure. The first and the third absorption bands are induced by the fundamental and the third-harmonic magnetic resonances, respectively, and the second absorption band between the first and the third ones appears by the magnetic resonance separated by two grooves on both sides of the disk. We also realize the triple absorption band even in the infrared and the visible regimes.

2. Simulation and experimental set-up

The simple design of MMPA, whose unit cell includes the toothed-wheel type at the front and a metallic plane at the back, separated by a dielectric substrate, is depicted schematically in Fig. 1(a) and (b). The geometrical parameters of triple-band absorption in the microwave range are selected to be $p = 19$, $r = 6.5$, $h = 5.5$ and $w = 0.8$ mm, and the substrate is FR4 with a thickness of 0.8 mm, together with a copper layer of 35 μm thick. The selected metal is the copper with an electric conductivity of 5.8×10^7 S/m, and the selected dielectric layer is FR-4 with a dielectric constant of 4.1 and a loss tangent of 0.02. The simulation has been carried out

* Corresponding author.
E-mail address: yplee@hanyang.ac.kr (Y. Lee).

http://dx.doi.org/10.1016/j.cap.2017.06.009

by a commercial software, CST Microwave Studio, which is based on the finite-element method. In the boundary condition, the direction of propagation (k) and the E-H field are z direction opened and x-y plane fixed, respectively. The EM-wave reflection [$R(\omega)$] and transmission [$T(\omega)$] of the scattering parameters are $|S_{11}(\omega)|^2$ and $|S_{21}(\omega)|^2$, respectively. The absorption [$A(\omega)$] is defined as $A(\omega) = 1 - R(\omega) - T(\omega) = 1 - |S_{11}(\omega)|^2 - |S_{21}(\omega)|^2$. Because the transmission is equal to be 0 by the continuous metallic plane, the absorption is recalculated by $A(\omega) = 1 - |S_{11}(\omega)|^2$. Fig. 1(c) and (d) present the fabricated sample of triple-band MMPA and the measurement set-up. The sample with a size of the 150×300 mm^2 was fabricated by the conventional photolithography process. In a microwave anechoic chamber, two linearly-polarized microwave standard-gain horn antennas, which were employed for transmitting the incident EM wave on the sample and for receiving the reflected EM wave from the sample, were connected to a Hewlett-Packard E8362B network analyzer by two connectors. The sample was set on a sample holder and located at a proper distance of 2.0 m from the middle of two horn antennas with an incident angle of 5° to the center of sample in order to avoid the interference effect between incident and reflected EM waves. We employed the copper plate of the same size for calibration in order to get the reference perfect-reflection spectrum and changed it to the fabricated sample for measuring the absorption.

3. Results and discussion

Fig. 2(a) and (b) display the simulated results of proposed structure to grasp change of the absorption spectrum at an incident angle of 5° for TE polarization according to the length h of two grooves from 0 to 5.5 mm. The lower-frequency peak (an absorption of 87.9% at 6.37 GHz) is induced by the fundamental magnetic response and the other peak (an absorption of 97.6% at 17.72 GHz) results from the third harmonic at $h = 0$ [20]. From $h = 2.5$ mm, another absorption peak between the lower-frequency and the higher-frequency bands grows and red-shifts by increasing the length of two grooves. At $h = 5.5$ mm, the triple bands reveal nearly-perfect absorption, with absorption of 98.22% at 4.89 GHz, 99.07% at 11.08 GHz and 98.3% at 17.29 GHz, and a minor absorption peak at 14.58 GHz with an absorption of 11.75% between the 2nd and the 3rd high absorption peaks. In order to demonstrate occurrence of the minor absorption peak, Fig. 2(c) shows the absorption plotted in a two-dimensional domain of the incident angle for TE mode at $h = 5.5$ mm. The overall absorption peaks are slightly red-shifted and another absorption peak occurs by increasing the incident angle. At an incident angle of 30°, we can particularly verify four absorption peaks at 4.92, 11.09, 14.31 and 17.66 GHz with absorption of 96.44%, 99.08%, 96.97% and 94.71%, respectively.

Fig. 3(a) shows comparison between simulation and experiment in the 4–18 GHz range for $h = 5.5$ mm. The experimental peaks (the 1st peak: 4.8 GHz, the 2nd peak: 11.28 GHz, and the 3rd peak: 17.51 GHz) are coincident with the simulation result (the 1st peak at 4.89 GHz, the 2nd peak at 11.08 GHz, and the 3rd peak at 17.29 GHz). The resonance frequencies of the absorption peaks according to the length of two grooves is analyzed in detail, as in Fig. 3(b). By increasing the h value, all the absorption peaks show red-shift. Especially, the 2nd absorption peak turns out to be more red-shifted than the other peaks. In the previous research, a significant portion of surface current at the 1st peak flows along the edge of disk, while a large amount of surface current at the 3rd peak flows in the inner area of disk [20]. The 2nd absorption peak appears by the surface currents which are separated between the upper and the lower metallic pattern parts, and the 2nd absorption peak cannot be observed until $h = 1.5$ mm owing to the inadequate

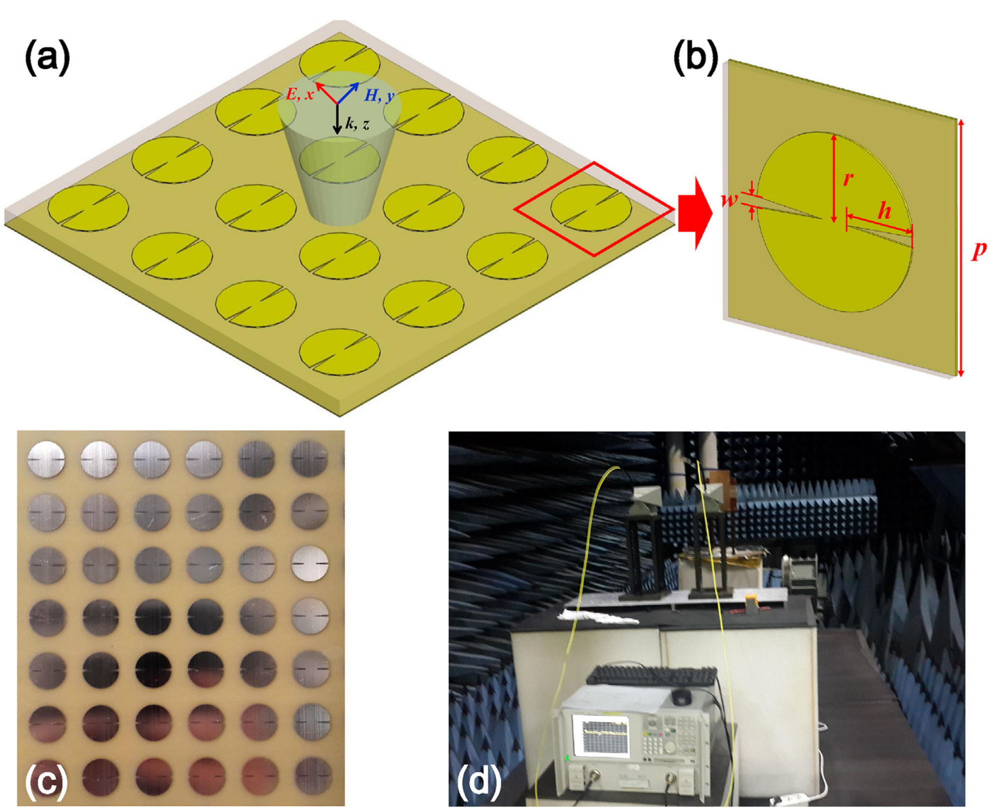

Fig. 1. (a) Schematic diagram of the MMPA and the unit cell, and (b) side view of the unit cell of MMPA. Photos of (c) the fabricated sample and (d) the measurement set-up.

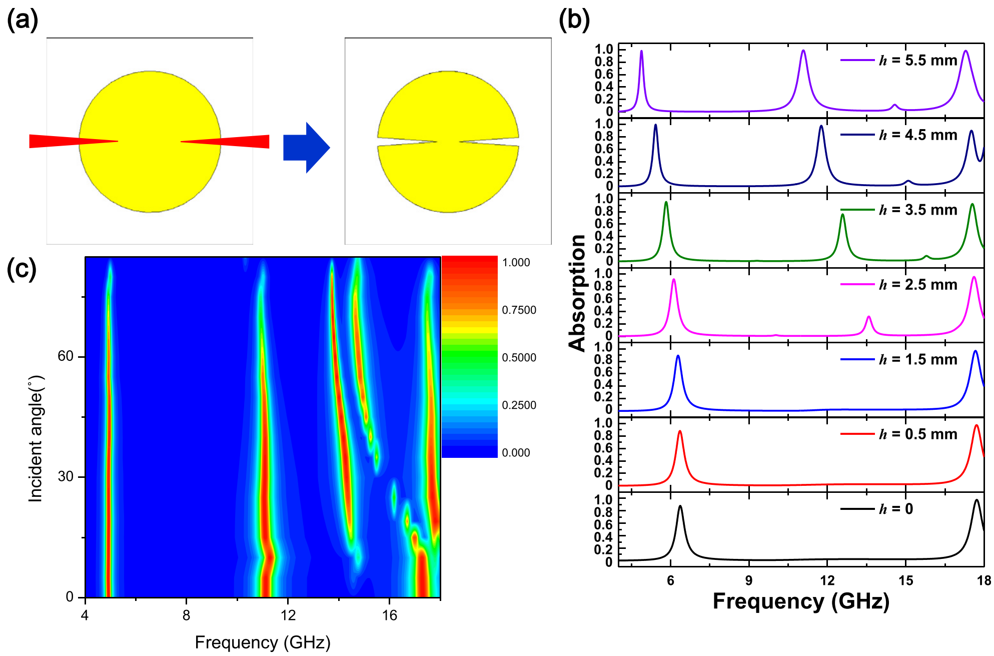

Fig. 2. (a) Schematic diagram of the single unit cell with two grooves, and (b) simulated absorption spectra for the proposed structure, depending on the length *h* of two grooves in 4–18 GHz. (c) Dependence of the simulated absorption spectra on the incident angle for TE mode.

length of two grooves for separation of the surface currents between the upper and the lower ones. For better understanding, we employ the surface-current distribution for each resonance frequency at $h = 5.5$ mm in Fig. 3(c). The surface currents at the 1st peak flows like the fundamental magnetic resonance, and those at the 3rd peak flows like the third harmonic magnetic resonance.

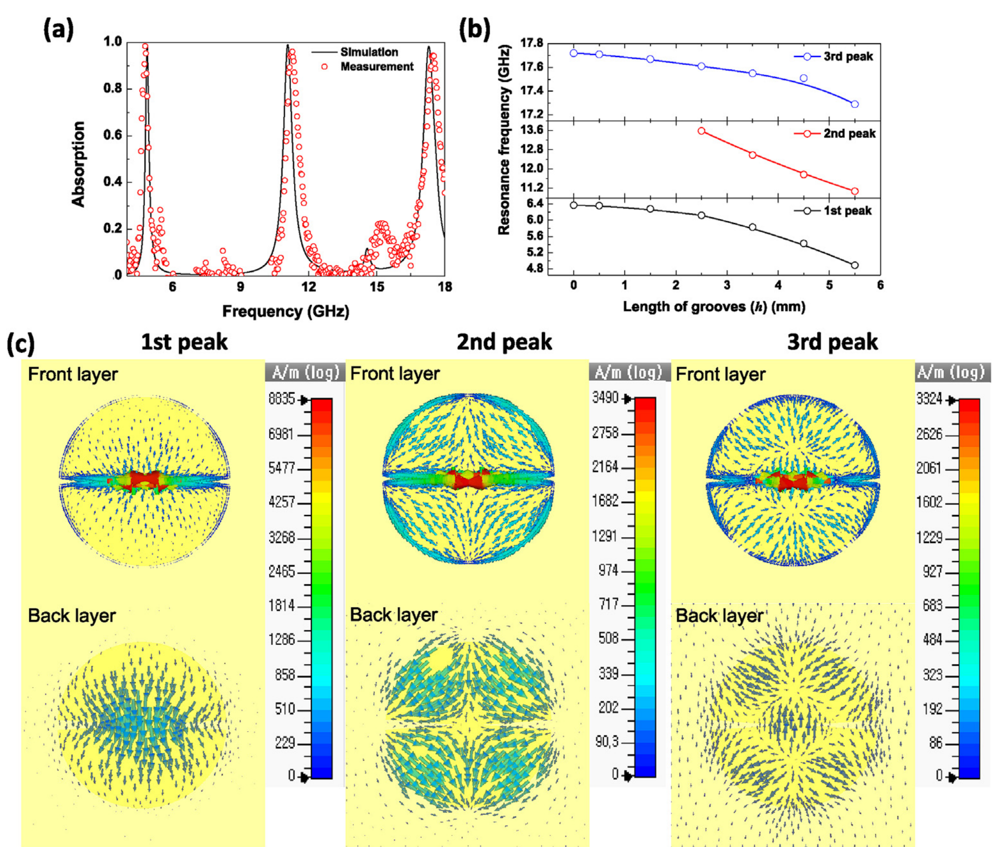

Fig. 3. (a) Simulated and measured absorption spectra for the proposed structure at $h = 5.5$ mm, and (b) resonance frequencies for the 1st, the 2nd and the 3rd peaks according to *h*. (c) Distribution of the induced surface currents for $h = 5.5$ mm in the metallic pattern (up) and the continuous metallic plane (down) at the 1st, the 2nd and the 3rd peaks.

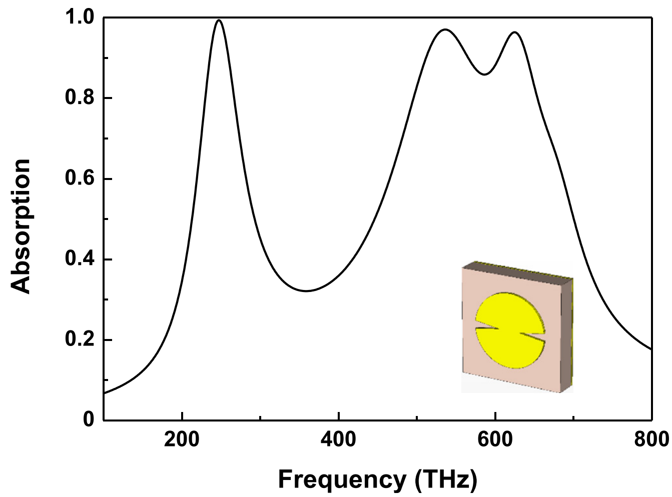

Fig. 4. Simulated absorption spectrum of the MMPA for triple-band perfect absorber working in the visible range.

However, the surface currents at the 2nd peak flows separately in the upper and the lower parts. In the equivalent oscillating-current resonant circuit, the effective inductance (L_m) of front and back metallic layers for the 1st peak can be approximately derived by

$$L_m = 4\mu_0 t \arccos\frac{w}{2r} + \frac{4\mu_0 t}{r-h}\ln r \tag{1}$$

and the effective capacitance (C_m) for the 1st peak by the interaction between metallic pattern layer and continuous metallic plane can be expressed by Ref. [21].

$$C_m = \frac{\varepsilon\varepsilon_0 c_1}{t}\left[\pi r^2 - hw\right] \tag{2}$$

Here, t and is the thickness of the dielectric layer, and r, w and h are the geometric parameters in Fig. 1. μ_0, ε_0, ε and c_1 are the magnetic permeability and the electric permittivity of the free space, a dielectric constant of FR-4, and a numerical factor, respectively. The resonance frequency is defined by $f_m = 1/[2\pi(L_m C_m)^{1/2}]$, and the resonance frequencies show red-shift according to h, due to the fact that the inductance increases by increasing the length of two grooves. The effective inductance and the effective capacitance for the 2nd peak are a half of L_m and C_m.

We simulated the absorption spectrum by reducing the geometrical parameters, since the proposed structure is applied not only for the microwave regime but also for the infrared and the visible ones (Fig. 4). The geometrical parameters of triple-band absorption for the infrared and the visible ranges are selected to be $p = 200$, $r = 70$, $h = 49$ and $w = 15$ nm, and the substrate is silicon with a thickness of 40 nm, together with a gold back layer of 5 nm thick. Three resonance peaks show nearly wide-band perfect absorption of 99.38% at 247 THz, 97.05% at 536 THz, and 96.79% at 625 THz. In the proposed MMPA for the visible range, the 2nd and the 3rd absorption peaks can be connected by adjusting the length of two grooves, which is also applied to the microwave range.

4. Conclusions

In conclusion, we designed and fabricated the triple-band MM absorber utilizing the toothed-wheel structure. The experiment has been performed, based on the simulation results in 4–18 GHz, and we compared elaborately the spectra of simulation and measurement. It was understood how high absorption for triple bands is achieved and the origin of the red-shift of resonance frequencies has been explained by using the distribution of surface currents. In addition, the MMPA for triple-band perfect absorption working in the infrared and the visible regimes was realized with similar but smaller unit cells.

Acknowledgment

This work was supported by the ICT R&D Program of MSIP/IITP, Korea (2013-0-00375) and by the NRF funded by MSIP, Korea (No. 2017R1A2B4003916).

References

[1] F.J. Garcia-Vidal, L. Martin-Moreno, J.B. Pendry, J. Opt. A, Pure Appl. Opt. 7 (2005) S97.
[2] S. Lan, L. Kang, D.T. Schoen, S.P. Rodrigues, Y. Cui, M.L. Brongersma, W. Cai, Nat. Mater. 14 (2015) 807.
[3] D. Schurig, J.J. Mock, B.J. Justice, S.A. Cummer, J.B. Pendry, A.F. Starr, D.R. Smith, Science 314 (2006) 977.
[4] A.K. Iyera, G.V. Eleftheriades, Appl. Phys. Lett. 92 (2008) 131105.
[5] D. Shrekenhamer, W. Xu, S. Venkatesh, D. Schurig, S. Sonkusale, W. Padilla, Phys. Rev. Lett. 109 (2012) 177401.
[6] H. Zhu, F. Yi, E. Cubukcu, Nat. Phot. 10 (2016) 709.
[7] L. Cong, S. Tan, R. Yahiaoui, F. Yan, W. Zhang, R. Singh, Appl. Phys. Lett. 106 (2015) 031107.
[8] J. Grant, I.J.H. McCrindle, D.R.S. Cumming, Opt. Express 24 (2016) 3451.
[9] H. Wang, V.P. Sivan, A. Mitchell, G. Rosengarten, P. Phelan, L. Wang, Sol. Energy Mater. Sol. Cells 137 (2015) 235.
[10] N. Liu, M. Mesch, T. Weiss, M. Hentschel, H. Giessen, Nano Lett. 10 (2010) 2342.
[11] W. Ma, D. Jia, Y. Wen, X. Yu, Y. Feng, Y. Zhao, Opt. Lett. 41 (2016) 2974.
[12] J.L. Perchec, Y. Desieres, N. Rochat, R.E. de Lamaestre, Appl. Phys. Lett. 100 (2012) 113305.
[13] N.I. Landy, S. Sajuyigbe, J.J. Mock, D.R. Smith, W.J. Padilla, Phys. Rev. Lett. 100 (2008) 207402.
[14] Y. Ma, Q. Chen, J. Grant, S.C. Saha, A. Khalid, D.R.S. Cumming, Opt. Lett. 36 (2011) 945.
[15] X. Shen, Y. Yang, Y. Zang, J. Gu, J. Han, W. Zhang, T.J. Cui, Appl. Phys. Lett. 101 (2012) 154102.
[16] Y.J. Kim, Y.J. Yoo, K.W. Kim, J.Y. Rhee, Y.H. Kim, Y.P. Lee, Opt. Express 23 (4) (2015) 3861.
[17] Y.J. Kim, J.M. Kim, Y.J. Yoo, P.V. Tuong, H. Zheng, J.Y. Rhee, Y.P. Lee, J. Opt. Soc. Am. B 31 (2014) 2744.
[18] J.W. Park, P.V. Tuong, J.Y. Rhee, K.W. Kim, W.H. Jang, E.H. Choi, L.Y. Chen, Y.P. Lee, Opt. Express 21 (2013) 9691.
[19] F. Dincer, M. Karaaslan, E. Unal, O. Akgol, C. Sabah, J. Electron. Mater. 43 (2014) 3949.
[20] Y.J. Yoo, Y.J. Kim, P.V. Tuong, J.Y. Rhee, K.W. Kim, W.H. Jang, Y.H. Kim, H. Cheong, Y.P. Lee, Opt. Express 21 (2013) 32484.
[21] J. Zhou, E.N. Economon, T. Koschny, C.M. Soukoulis, Opt. Lett. 31 (2006) 3620.